Explicit symmetry breaking of generalized angular momentum by second-harmonic generation in underdense plasmas

Alexis Voisine, P. Béjot, Franck Billard, Hugo Marroux, Olivier Faucher, Edouard Hertz

Abstract Light beams possess two intrinsic quantized degrees of freedom, related to spin angular momentum (SAM) and orbital angular momentum (OAM), whose manipulation enables extensive control over the topological properties of electromagnetic fields. In this context, structured fields constructed from a non-separable combination of SAM and OAM have recently gained sustained interest. Such states are eigenstates of the so-called generalized angular momentum (GAM), a mixed angular momentum operator encompassing both SAM and OAM components, which can result in astonishing fractional eigenvalues. The demonstration of GAM conservation under harmonic generation has suggested a potential relevance of this new form of angular momentum as a meaningful quantum number. In the present work, we expand the scope of evaluation by investigating its conservation law with second-harmonic generation in an underdense isotropic inhomogeneous plasma that relies on dipole-forbidden interaction implying spin-orbit coupling. Our study reveals that the symmetry and topological properties of the field are disrupted during the nonlinear process, the GAM charge being only conserved on average. This symmetry breaking can be exploited to provide an easily detectable signature of the driving field topology or to create a robust topological attractor.

Explicit symmetry breaking of generalized angular momentum by second-harmonic generation in underdense plasmas

Alexis Voisine[†], Pierre Béjot[†], Franck Billard[†], Hugo Marroux[‡], Olivier Faucher[†] and Edouard Hertz[†,*]

1. Introduction

Angular momentum (AM) has unveiled unexpected phenomena in the field of optics whose the prominent facet was conventionally associated with the Spin Angular Momentum (SAM) related to the vectorial nature of the electromagnetic field. [1] However, since the seminal works of Allen, [2] it became apparent that electromagnetic waves with a twisted wavefront can also carry an orbital angular momentum (OAM). Shortly after this discovery, it was shown [3] that the SAM associated with circularly polarized light can add to, or subtract from, the OAM to give a total angular momentum (TAM). As a result, the TAM of light J_{photon} can write in its canonical form $J_{\text{photon}} = S_{\text{photon}} + L_{\text{photon}}$, in which the TAM is split into a spin and an orbital part. This description into two distinct quantities has nevertheless immediately raised deep questions on how to correctly define both SAM and OAM in a gauge-invariant manner. [4,5] In particular, for the general case of three-dimensional field, only the TAM $J_z = S_z + L_z$ constitutes a genuine angular momentum unlike S_z or L_z taken individually that fails to preserve the transversality of the electromagnetic field. The decomposition into spin and orbital angular momenta is in fact solely valid under the paraxial approximation [6] for which individual photons may carry discrete units of OAM and/or SAM. Furthermore, the AM is intimately linked to dynamic rotation property. Since the works of Emmy Noether, [7] it is well known that symmetry, invariance, and conservation principles are intrinsically linked, any differential symmetry being associated to a conservation law. The AM of an electromagnetic field is thus expected to be conserved during the propagation through a medium exhibiting a cylindrical symmetry. This fundamental property applies however for the TAM but not for SAM nor for the OAM separately. As a result, both kinds of momenta can couple in appropriate conditions. This phenomenon called spin-orbit coupling (SOC) of light [8,9] has triggered an intense research activity called *spinoptics* inspired by the spintronics of electronic systems. The potentialities opened by OAM and TAM have garnered significant attention in various fields [10,11] such as microscopy, [12] chirality, [13,14] quantum information processing, [15–19] optical tweezer, [3,20] and optical communications [21–24] while spin-orbit interactions have been examined for instance through second harmonic generation (SHG) produced in nonlinear crystals [25,26] or metasurfaces. [27] From a mathematical point of view, the AM operators are the infinitesimal generators of rotations that can act on an electromagnetic field. While the SAM operator, involving the third Pauli matrix $S_z = \sigma_3$, rotates the light polarization direction, the OAM operator, taking the form $L_z = -i\partial_\theta$ in cylindrical coordinates, leads to beam transverse profile rotation. The eigenstates of the SAM operator are the left $|\sigma_+\rangle$ and right $|\sigma_-\rangle$ circularly polarized beams, with eigenvalues $s = 1$ and $s = -1$ (in units of $\hbar$) respectively. Those of L_z correspond to beams whose spatial amplitude varies as $e^{i\ell\theta}$, with eigenvalues ℓ ($\ell \in \mathbb{Z}$). Such beams then embed an helical wavefront, rotating ℓ times during the propagation over one wavelength. As far as the TAM $J_z = L_z + S_z$ operator is concerned, the functional expression of its eigenstates takes the general form $|\psi_\ell\rangle = e^{i\ell\theta}\left[a_+(r)|\sigma_+\rangle + a_-(r)e^{2i\theta}|\sigma_-\rangle\right]$, with corre-

[†] Laboratoire Interdisciplinaire Carnot de Bourgogne, UMR 6303 CNRS-Université de Bourgogne, 21078 Dijon Cedex, France
[‡] Université Paris-Saclay, CEA, CNRS, LIDYL, 91191 Gif-sur-Yvette, France
[*] Corresponding author: e-mail: edouard.hertz@u-bourgogne.fr

sponding eigenvalues $j_\ell = \ell + 1$ that takes integer values in line with the fact that photons are classified as bosons. Note that this expression only relates to the transverse part of the field, the longitudinal component being given by the Maxwell-Gauss equation.

Few years ago, paraxial lights embedding a new form of angular momentum have been identified. [28] These light beams, built from a coherent non-separable superposition of SAM and OAM, feature non-trivial topologies. They are invariant under a transformation called *coordinated rotations*, a differential symmetry operation that rotates the spatial dependence of the electromagnetic field by an angle θ followed by a rotation of its polarization by an amount $\gamma\theta$. Such coordinated rotations are generated by the operator $J_{z,\gamma} = L_z + \gamma S_z$, called generalized angular momentum (GAM). For monochromatic waves, the coordination parameter γ takes either integer or half-integer values associated to the topology of twisted ribbons and Möbius strips, respectively. [29] When γ is half-integer, the GAM charge j_γ (eigenvalue of $J_{z,\gamma}$) is also half-integer with an unexpected fermionic-like spectrum. This astonishing quantization of AM is in fact related to the constrained symmetry associated with the paraxial nature of light beams and turns out to be a general characteristic of quantum systems with a reduced degree of freedom observed for instance with electrons orbiting in two-dimensions. [30] For polychromatic fields, the situation can be even more exotic with the possibility of any arbitrary rational j_γ values and nontrivial torus-knot topologies. [31]

The identification of this new form of fractional angular momentum has raised the issue of its physical significance and of its conservation through light-matter interaction. While it has been established that the TAM of light is conserved through up-conversion processes in isotropic circularly symmetric media, [32,33] one can wonder if the same holds for light beams owing a fractional angular momentum. In this context, the conservation law and potential transfer of topological properties from driving fields to up-converted photons have been examined in the realm of high harmonic generation (HHG) in atomic gas systems. Harmonics driven by fields invariant under coordinated rotation have theoretically revealed [34,35] a linear scaling of the harmonic GAM charge $j_\gamma^{(q)}$ with the harmonic order q (namely $j_\gamma^{(q)} = q j_\gamma$). This prediction was subsequently confirmed by analyzing the HHG induced by polarization Möbius strips [36] through a specific experimental scheme. The conservation of GAM in nonlinear optics suggests that, in addition to TAM, GAM may constitute a relevant quantum number. In these studies, the optical OAM and SAM were conserved independently. More particularly, the nonlinear process was generated in an isotropic and homogeneous medium under paraxial illumination through dipolar transitions, a physical configuration in which no spin-orbit coupling is expected. Indeed, light–matter interactions can engage the OAM content solely when multipolar transitions are at play. [13] This can be easily understood by remembering that the OAM feature of a beam is contained in the transverse variation of its spatial phase, while dipolar transitions are intrinsically purely local (i.e., the dipolar transition probability between two states depends solely on the value of the electric field at the exact position of the center of mass of the system). The first term in the multipolar expansion having the ability to engage the OAM content is the electric quadrupole interactions, which depends on the transverse gradients of the electric field. Quadrupolar interactions can thus mediate an OAM exchange between helical light and matter (in addition to SAM), allowing transitions otherwise forbidden as a result of SOC. This has been recently confirmed, for instance, by observing modifications of selection rules induced by the OAM of light in $^{40}Ca^{+}$ ions [37], nonlinear helical dichroism in liquid phase [14], or by measuring orbital photogalvanic effect in a Weil semimetal. [38] It is important to note that multipolar transitions can arise from two distinct physical origins, one taking into account the finite size of molecules (or atoms), the other one originating from the non-homogeneous distribution of the molecules in space. In the context of light invariant by coordinated rotation, changes in selection rules due to SOC are expected to modify the conservation law of GAM charge opening rich scenarios of study with potential explicit symmetry breaking. It therefore offers an expanded scope of evaluation and provides further insights into the relevance of the GAM as an appropriate quantum number. In this paper, we examine the conservation law of GAM when up-converted photons are produced through a dipole-forbidden, quadrupole-allowed interaction. The corresponding nonlinear process involves second-harmonic generation (SHG) produced in an isotropic but radially inhomogenous plasma, a configuration known to produce even harmonics despite the centro-symmetric nature of the medium. The two current source terms of SHG can be identified as magnetic dipole and electric quadrupole contributions, [39] while no electric dipole polarization exists. In this case, the plasma does no retain any angular momentum from the beam, akin to HHG, but simply acts as a catalyst where the TAM is conserved but with potential SOC. [33] This well-understood nonlinear excitation process thus constitutes an attractive platform for testing the conservation law of angular momentum and observing a potential symmetry breaking of GAM. As shown below, while dipole-allowed HHG process only allows two quantum channels (for a given harmonic order) when driven by a coordinated rotation invariant light, quadrupole-allowed SHG gives rise to four distinct quantum channels. Analysis of these various pathways requires a phase-matching free interaction, which is obtained in this study by using an ultra-thin flat leaf of liquid water as nonlinear medium. [40] Based on this configuration, the symmetry and topological properties of the GAM state is shown to be broken during the nonlinear process, the GAM charge being nevertheless conserved *on average*. This effect can be explained by the quantum interferences between different excitation paths which plays a crucial role in the SOC mode of the generated harmonic field. [41] We demonstrate that the symmetry breaking enables a straightforward identification of the driving field topology whose signature is encoded into the spatial amplitude of the SHG field. Finally, it is anticipated that, if isolated, specific quantum pathways behave as a topological attractor for the harmonic field.

2. Generalized Angular Momentum

We consider in the following an electric field whose transverse part writes in cylindrical coordinates as:

$$|\psi\rangle = a_+ e^{i\ell_+\theta}|\sigma_+\rangle + a_- e^{i\ell_-\theta}|\sigma_-\rangle, \tag{1}$$

where $|a_+|^2+|a_-|^2 = 1$ and $|\sigma_\pm\rangle = (1, \pm i)$. Introducing $\gamma = \frac{\ell_- - \ell_+}{2}$ the coordination parameter, it can be easily seen that $|\psi\rangle$ is eigenstate of the GAM operator $J_{z,\gamma} = L_z + \gamma S_z$ with the eigenvalue $j_\gamma = \frac{\ell_- + \ell_+}{2}$. Note that $|\psi\rangle$ is not eigenstate of either L_z or S_z. For γ=1, we recover the usual eigenstates of the TAM operator $J_z = L_z + S_z$ (note that $J_{z,1}$ is written J_z in the following to simplify the notation). The operator $J_{z,\gamma}$ is an infinitesimal generator of coordinated rotation of field amplitude and polarization whose eigenstates feature non-trivial topologies. More particularly, the corresponding fields are invariant, up to a phase factor $e^{ij_\gamma\theta}$, to the coordinated rotations (CR) which consists in rotating the spatial field by an angle θ followed by a rotation of its polarization by $\gamma\theta$. Such beams of spatially varying polarization distribution are commonly referred to as CR-invariant beams. [35] As an example, Fig. 1(a) depicts an eigenstate of $J_{z,1/2}$ with the corresponding eigenvalue $j_{1/2} = 1/2$ that takes the functional form $|\psi\rangle^{\gamma=1/2}_{j_{1/2}=1/2} = \frac{|\sigma_+\rangle + e^{i\theta}|\sigma_-\rangle}{\sqrt{2}}$. The corresponding coordination factor $\gamma = 1/2$ is half-integer leading to a so-called polarization Möbius strips. As exemplified in Fig. 1(b), any other eigenstate of the same operator $J_{z,1/2}$ but with a different eigenvalue shares the same topology although with distinct azimuthal phase. This can be readily understood by recasting the field state of Eq. 1 with the relation

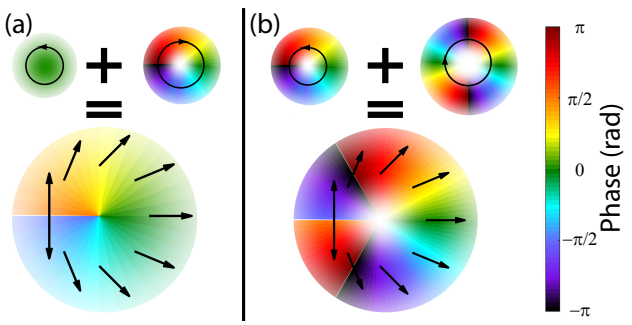

Figure 1 Schematic representation of eigenstates of $J_{z,1/2}$. The corresponding eigenvalue is $j_{1/2} = 1/2$ for (a) and $j_{1/2} = 3/2$ for (b). The upper part depicts the decomposition along the two polarization components with the spatial phase in colormap.

$$\ell_\pm = j_\gamma \mp \gamma, \tag{2}$$

giving:

$$|\psi\rangle^{\gamma}_{j_\gamma} = e^{ij_\gamma\theta}\left(a_+ e^{-i\gamma\theta}|\sigma_+\rangle + a_- e^{i\gamma\theta}|\sigma_-\rangle\right). \tag{3}$$

As a result, the electric field at any point in the transverse coordinate (r,θ) will exhibit a polarization state which depends on the term in parentheses and therefore on γ and $a_\pm$ but not on j_γ which induces an azimuthal phase. Finally, while $a_\pm$ in Eq. 3 can be complex, we point out that any phase term $e^{i\phi}$ applied to the $|\sigma_\pm\rangle$ component results in a global rotation of the polarization pattern (Fig. 1) by an angle $\theta_0 = \pm\frac{\phi}{2}$.

3. SHG from plasma currents and angular momentum conservation

In an inhomogeneous plasma, the second-harmonic generation process comes from the fact that both velocity and charge distribution (although the net charge distribution of the plasma with no field is null) oscillate in time at the field frequency. As a result, since the current is the product of both quantities, the latter will embed a (small) component oscillating at twice the field frequency. More particularly, let us consider an isotropic non-magnetic medium of linear susceptibility $\chi^{(1)}$ (supposed constant with the frequency and homogeneous in space to simplify). In this case, the Maxwell's equations in presence of a low-density plasma read:

$$\begin{aligned} \nabla\times\vec{E} &= -\partial_t\vec{B} & \nabla\cdot\vec{D} &= \rho \\ \nabla\times\vec{B} &= \mu_0\left(\vec{J}_c + \partial_t\vec{D}\right) & \nabla\cdot\vec{B} &= 0, \end{aligned} \tag{4}$$

where μ_0 is the vacuum permeability, $\vec{E}$ and $\vec{B}$ are the real electric and magnetic fields respectively, and ρ is the total charge density distribution. The constitutive equation linking the electric field to the displacement field $\vec{D}$ reads

$$\vec{D} = \epsilon_0 n^2 \vec{E}, \tag{5}$$

where $n = \sqrt{1+\chi^{(1)}}$ is the refractive index and ϵ_0 the vacuum permittivity, while the charge conservation equation reads:

$$\nabla\cdot\vec{J}_c + \partial_t\rho = 0, \tag{6}$$

where $\vec{J}_c = \rho_e\vec{v}_e$ is the current induced by the free electron (ions are supposed to remain at rest), ρ_e is the electron charge distribution, and $\vec{v}_e$ is the electron velocity. In presence of an electromagnetic field, the latter is driven by the momentum equation:

$$m_e\left[\partial_t\vec{v}_e + (\vec{v}_e\cdot\nabla)\vec{v}_e\right] = q_e\left(\vec{E} + \vec{v}_e\wedge\vec{B}\right), \tag{7}$$

where q_e and m_e are the electron charge and mass, respectively. The plasma is supposed to be initially neutral and the electrons initially at rest so that: $\rho(\vec{r}, t=0) = \rho_{\text{ions}}(\vec{r}, t=0) + \rho_e(\vec{r}, t=0) = 0$. Since the ions remains at rest, it implies for the charge density:

$$\rho(\vec{r}, t) = \rho_e(\vec{r}, t) - \rho_e(\vec{r}, t=0). \tag{8}$$

Using the equations above and decomposing the current $\vec{J}_c$, the charge distribution ρ and the electron velocity $\vec{v}_e$ as Fourier series in frequency, one finds the expression of the

current contribution oscillating at twice the field frequency ω_0:

$$\vec{J}_c^{2\omega_0} = \frac{iq_e^3}{m_e^2\omega_0^3}\left[\frac{n_e^{(0)}}{4}\nabla\left(\vec{E}\cdot\vec{E}\right) + \frac{\left(n^2\nabla n_e^{(0)}\cdot\vec{E}\right)}{n^2-\frac{n_e^{(0)}}{n_c}}\vec{E}\right], \quad (9)$$

where $n_e^{(0)}$ is the electron density and $n_c = \frac{\epsilon_0 m_e \omega_0^2}{q_e^2}$ is the critical electron density. In the paraxial regime, the first term in Eq. 9 will be mainly longitudinal (i.e., along z), so that it cannot radiate in the propagation direction. As a result, the second-harmonic generation in the bulk of a nonuniform plasma is only possible through the second term in Eq. 9. In the case of a circularly symmetric inhomogeneous plasma [$n_e = n_e(r)$], the second-harmonic current will then be of the following functional form:

$$\vec{J}_c^{2\omega_0} \propto \left(\vec{E}\cdot\vec{e}_r\right)\vec{E}, \quad (10)$$

revealing that the SHG field owns the same polarization as the pump field. The expression of plasma-induced SHG for any fundamental driving field can be deduced from Eq. 10. In particular, using the fact that circular polarizations $|\sigma_\pm\rangle = (1, \pm i)$ writes as $|\sigma_\pm\rangle = e^{\pm i\theta}(\vec{e}_r \pm i\vec{e}_\theta)$ in cylindrical coordinates, one finds [see Section 3, Supporting information] that the CR-invariant field of Eq. 3, eigenstate of the GAM operator $J_{z,\gamma}$, generates a SHG field writing as:

$$\begin{aligned}\vec{E}^{2\omega_0} \propto\ & e^{i(2j_\gamma-\gamma+1)\theta}\left(a_+^2 e^{-i\gamma\theta}|\sigma_+\rangle + a_+a_- e^{i\gamma\theta}|\sigma_-\rangle\right)\\ & + e^{i(2j_\gamma+\gamma-1)\theta}\left(a_-a_+ e^{-i\gamma\theta}|\sigma_+\rangle + a_-^2 e^{i\gamma\theta}|\sigma_-\rangle\right)\end{aligned} \quad (11)$$

where one can easily recognize the superposition of two eigenstates of the GAM operator $J_{z,\gamma}$ with different eigenvalues $j_\gamma^{2\omega_0} = 2j_\gamma - \gamma + 1$ and $j_\gamma^{\prime 2\omega_0} = 2j_\gamma + \gamma - 1$:

$$\vec{E}^{2\omega_0} \propto |\psi\rangle^{\gamma}_{j_\gamma^{2\omega_0}} + |\psi\rangle^{\gamma}_{j_\gamma^{\prime 2\omega_0}}. \quad (12)$$

We emphasize that the two GAM states of this coherent superposition are both eigenstates of the GAM operator $J_{z,\gamma}$ (like the fundamental field) indicating that the topology of the driving field has been transferred to each of them during the nonlinear process.

The previous analysis enables the anticipation of all the various scenarios addressed in this study, from the simplest to the most comprehensive. For instance, the SHG driven by a pure helically phased field $|\psi\rangle = e^{i\ell_+\theta}|\sigma_+\rangle$ can be deduced from Eq. 11 by setting $a_+ = 1$ and $a_- = 0$. The SHG field then writes as:

$$\vec{E}^{2\omega_0} \propto e^{i(2(j_\gamma-\gamma)+1)\theta}|\sigma_+\rangle = e^{i(2\ell_++1)\theta}|\sigma_+\rangle \quad (13)$$

where the relation $\ell_+ = j_\gamma - \gamma$ (Eq. 2) has been used to derive the last formulation. As previously mentioned, the SHG field owns the same polarization as the pump field, thereby imposing a spin selection rule. Furthermore, while the input field $|\psi\rangle$ is eigenvector of J_z with the eigenvalue $j^{\omega_0} = \ell_+ + 1$, the SHG field of Eq. 13 is also eigenvector of J_z with an eigenvalue $j^{2\omega_0} = 2j^{\omega_0}$, confirming therefore the conservation of the TAM during the plasma-induced SHG process. This effect, already observed in previous studies, [33,42] is a general rule for a current source with no dissipation is in fact a consequence of the Noether theorem since the plasma gradient is invariant under rotation around the propagation axis. This finding allows to derive general selection rules for a given SHG quantum channel which can be summarized as:

$$\begin{aligned}&\Delta j = j^{2\omega_0} - \sum_{i=1}^{2} j_i^{\omega_0} = 0\\ &|\sigma^{2\omega_0}\rangle = |\sigma^{\omega_0}\rangle.\end{aligned} \quad (14)$$

In the simple case of circularly polarized helically phased fields, the conservation laws rewrite $\Delta s = \mp 1$ and $\Delta\ell = \pm 1$ where neither the SAM nor the OAM are conserved during the process, which is a manifestation of spin-orbit coupling. The case of SHG driven by CR-invariant beams described by Eqs. 11-12 can be retrieved from theses rules considering the different pairs of photons in the input GAM state (Eq. 3) that can initiate the nonlinear process. SHG field in Eq. 11 involves a superposition of 4 quantum channels. The first channel (term of amplitude a_+^2) is driven by two photons of left helicity, the last one (of amplitude a_-^2) by two photons of right helicity, and the other two channels (of amplitude a_+a_-) corresponds to crossed channels produced by one photon from each polarization state. It can easily be shown [see Section 2, Supporting information] that the topological charge of each photon can be predicted through the upper conservation law. Consequently, while dipole-allowed HHG driven by monochromatic CR-invariant beams only allows two quantum channels resulting in a CR harmonic field with $j_\gamma^{q\omega_0} = q j_\gamma^{\omega_0}$ (where q is the harmonic order), SHG induced from plasma currents yields four distinct quantum channels resulting in the superposition of two CR harmonic fields of different eigenvalues (see Eq. 12).

Finally, another conservation rules has to be considered. Indeed, the translation invariance of the medium along the propagation implies conservation of the linear momentum during the nonlinear process. Experimentally speaking, all OAM fields under investigation can be described by Laguerre-Gauss modes LG_p^ℓ, that exhibit a ℓ and p-dependent Gouy phase. For simplicity, considering only the case p=0, the latter varies as $(|\ell|+1)\arctan(z/z_r)$, where z_r is the Rayleigh length. As a result, the production of second-harmonic from plasma is not necessarily phase-matched. The SHG process induced by pure OAM beam of topological charge ℓ (see for instance Eq. 13) is phase-matched only for $\ell s \geq 0$. Likewise, the efficiency of the different SHG channels when driven by CR-invariant beams (Eq. 11) will not be uniform as it is influenced by phase-matching considerations. Consequently, the overall signal resulting from their superposition may undergo a modification of its spatial structure, hampering direct comparison to theory. So as to study potential symmetry breaking at the microscopic level, analysis of nonlinear interactions with GAM states therefore requires a nonlinear medium of small thickness (overcoming

phase-matching issues). For this purpose, the SHG was generated within an ultra-thin flat leaf of liquid water. [40] It is noteworthy that this experimental configuration differs from earlier investigations [33,42] where the SHG field was generated in a static gas sample. These last indeed focused on SHG driven by pure OAM fields, where phase-matching predominantly influences the amplitude of the generated signal rather than its spatial structure, thus having minimal impact on qualitative analysis.

4. Experimental set-up

The experimental set-up is depicted in Fig. 2. The experiment is conducted with a Ti:Sa femtosecond laser delivering pulses centered at 802 nm at 1 kHz repetition rate and of duration 35 fs. The use of femtosecond laser pulses, due to their high peak intensity, is well-suited for the targeted analysis as they can generate significant plasma through non-resonant ionization. However, the conclusions of our study are not necessarily limited to interactions involving ultrashort laser pulses. The energy of the driving beam (called "Pump" in Fig. 2) is first controlled by a combination of half-waveplate (HWP) and polarizer (P). Its spatial structuring, so as to imprint OAM or GAM states, is achieved by a beam shaper built from the combination of waveplate(s) and q-plates that are used for generating OAM beams via SAM-OAM exchange occurring in both anisotropic and inhomogeneous media. [44] Depending on the shaping to produce, different combinations have been implemented [see Section 1, Supporting information]. After the beam shaper, the driving beam propagates through a band-pass filter centered at 800 nm so as to remove any possible contribution of second-harmonic field produced within the optics. The spatially shaped fundamental beam is then focused by a lens (L_1) of 25 cm focal length in the nonlinear medium for producing the SHG field through induced plasma. SHG signal is observable in air gas but as explained in the previous section, a thin water flat leaf is used as nonlinear medium so as to get rid of phase-matching limitations. This last is created via the collision of two laminar flow cylindrical jets. [40] To ensure stability and ease of alignment, the two cylindrical jets are engraved into a single microfluidic chip. The holder and tubing are made of PEEK for chemical stability and high-pressure handling. Typical flow speeds of 2.5 mL/min are used resulting in leaf thickness of a few microns. After the interaction, the SHG radiation is isolated from the fundamental field by a 400 nm band-pass filter, analyzed in polarization, via a Berek compensator (BC) and a polarizer, before being imaged on a CCD camera. The spatial phase of the beam is obtained by measuring the interference pattern with a frequency-doubled reference beam crossing at small angle (0.5°) and by performing a spatial Fourier filtering. [18]. The reference beam is spatially filtered by a focusing through a pinhole aperture of 30 μm diameter. Reference and driving fields are temporally synchronized using a translation stage. Measurements have been realized with a typical pump energy of few tens of μJ.

5. Experimental results

We first investigate the SHG produced from a pure circularly polarized field $|\sigma_+\rangle$ ($\ell = 0$). The selection rules in Eqs. 13-14 predicts in this case the production of harmonic photons polarized along $|\sigma_+\rangle$ and carrying the topological charge $\ell^{2\omega_0} = 1$. The SHG field, measured with our setup, is depicted in Fig. 3(a,b), where panels (a) and (b) correspond to the analysis along the left- and right-handed polarization components, respectively. A comparison of signal amplitudes reveals that the harmonic field displays the anticipated dominant $|\sigma_+\rangle$ circular polarization. Furthermore, the beam profile exhibits an annular intensity pattern which strongly suggests the presence of a phase singularity on the beam axis and the generation of an OAM beam through the nonlinear process. The reconstruction of the spatial phase [lower panel of Fig. 3(a)] confirms this prediction. The counter-clockwise winding from 0 to 2π of the phase distribution agrees with the expected helical phase structure $e^{i\theta}$. Similarly, the SHG field produced from a field of right circular polarization, depicted in Fig. 3(c,d), is found to be of the form $e^{-i\theta}|\sigma_-\rangle$. All these results are in excellent agreement with the findings previously reported in the literature. [33,42] The case of mixed state is first examined considering the simple case of a radially polarized field, eigenstate of J_z (i.e. $\gamma = 1$) and $j_\gamma = 0$, writing as $|\psi\rangle_0^1 = \frac{e^{-i\theta}|\sigma_+\rangle + e^{i\theta}|\sigma_-\rangle}{\sqrt{2}}$. The expected SHG field can be inferred from Eq. 11 which forecasts the production of a radially polarized field. The outcome, illustrated in Fig. 3(e,f), reveals a SHG field with two components of opposite helicities. The two components exhibit a nearly annular intensity distribution of equal amplitude and the retrieved phase shows opposite winding distribution with a single spiral arm, indicating a SHG field built from a superposition of $e^{-i\theta}|\sigma_+\rangle$ and $e^{i\theta}|\sigma_-\rangle$. The topology of the fundamental field is thus perfectly transferred to the harmonic field. Once again such a result is not surprising considering the conservation of the TAM predicted by the Noether's theorem.

We turn next to the central purpose of this paper, namely the SHG driven by CR-invariant fundamental field (of coordination parameters $\gamma \neq 1$). The first investigated case deals with the polarization Möbius strip of Fig. 1(a), namely $|\psi\rangle_{1/2}^{1/2} = \frac{|\sigma_+\rangle + e^{i\theta}|\sigma_-\rangle}{\sqrt{2}}$ (eigenstate of $J_{z,1/2}$ with the GAM charge $j_{1/2} = 1/2$). The SHG produced by such a field of spatially varying polarization can be anticipated through Eqs. 11-12. It can be shown that the resulting output SHG field can be recast with the following functional form:

$$\vec{E}^{2\omega_0} \propto e^{ij_\gamma\theta}\cos\left[(\gamma-1)\,\theta\right]\vec{E} \tag{15}$$

revealing that the output SHG field will exhibit a modulation of its amplitude. Any input field that is eigenstate of $J_{z,\gamma}$ with $\gamma \neq 1$) will therefore experience a symmetry breaking through SHG process. For the present case ($\gamma = 1/2$), the anticipated modulation is of the form $\cos[\theta/2]$. This can be qualitatively understood from the shape of the input field. According to Eq. 10, the signal will reach its maximum (minimum) for all spatial positions where the electric field

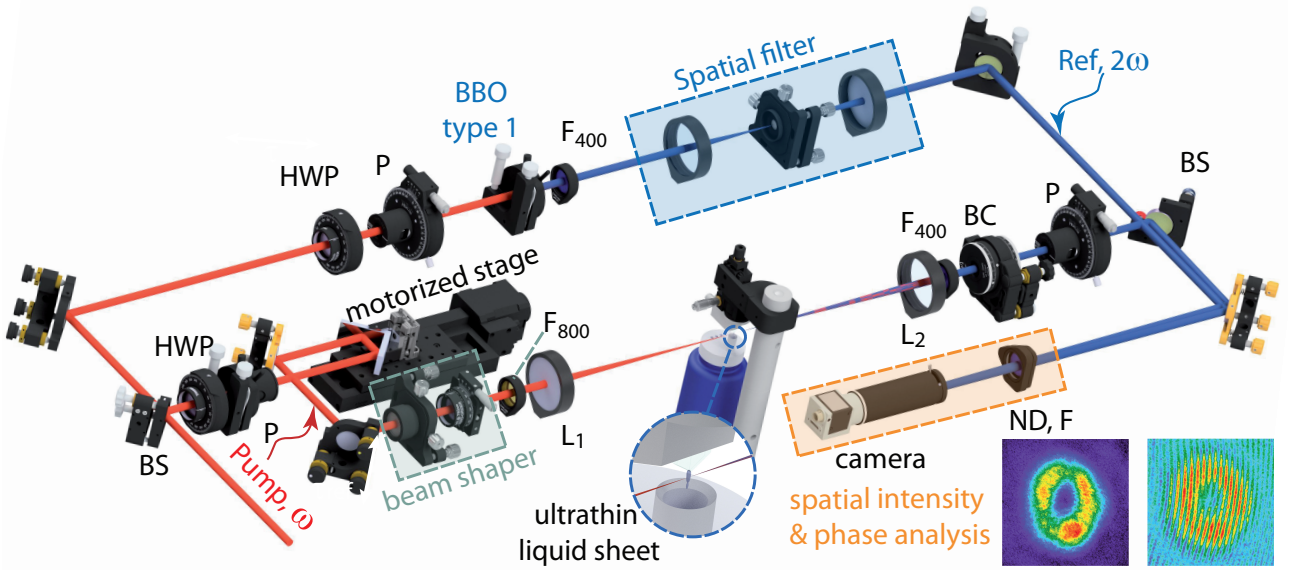

Figure 2 Experimental set-up. BS: beam splitter, HWP: half waveplate, P: polarizer, L: plano-convex lens, BC: Berek compensator, F_{800}/F_{400}: 800/400 nm bandpass filter, ND: neutral density, BBO: type 1 doubling.

points along the radial (orthoradial) direction. The field vector distribution shown in Fig. 1 therefore allows to foresee a maximum (resp. minimum) intensity for $\theta = 0$ (resp. $\theta = \pi$). This prediction is in line with the crescent-shaped intensity profile measured in Fig. 4. More specifically, this figure displays the SHG signal for varying longitudinal positions z of the liquid jet. As it can be seen, the harmonic beam profile consistently exhibits a crescent-shaped that rotates as the liquid leaf is moved away from the beam waist position. This effect arises because the two components of opposite helicities building the input state $|\psi\rangle$ carry topological charges of different absolute values $|\ell_+| \neq |\ell_-|$. These two components will therefore acquire a differential Gouy phase shift during their propagation leading to the rotation of the polarization pattern (Fig. 1), inducing therefore a rotation of the generated harmonic signal. This observation emphasizes the relevance of using a thin nonlinear medium for limiting phase-matching issues that could otherwise alter the spatial structure of signals and make its analysis more challenging. Let's proceed now with a more in-depth examination of the generated signal and its relation to the conservation of angular momentum. The amplitude and phase of the harmonic field along the two polarizations components are depicted in Fig. 5. Both components feature the same crescent-shaped intensity profile, consistent with Eq. 15. The spatial phase relies, for its part, on a complex modulation that integrates the azimuthal phase carried by $e^{ij_\gamma\theta}\vec{E}$ with the phase jump of the cosine amplitude modulation as outlined in Eq. 15. Although the final spatial phase can be challenging to assess, the experimental measurements [Figs. 5(a,b) and (e,f)] closely align with the simulation [Figs. 5(c,d) and (g,h)], supporting the validity of our modeling approach. The minor discrepancies with the experiment can be attributed to the production of vortex beams that are not pure Laguerre-Gauss modes (ℓ, p=0), resulting in variations in the divergence of the different components upon diffraction. [43] Nevertheless, the prominent result is that the output SHG is modulated in amplitude while the fundamental field is not, indicating a clear occurrence of GAM symmetry breaking. The SHG field in this case can be deduced from Eqs. 11-12 with the parameters $\gamma = 1/2$ and $j_{1/2} = 1/2$. From Eq. 12, one can see that the output SHG field writes as the superposition of two polarization Möbius strip fields both associated to the same coordination parameter $\gamma = 1/2$ but with different GAM charges $j_{1/2}^{2\omega_0} = 3/2$ and $j_{1/2}^{\prime 2\omega_0} = 1/2$:

$$\vec{E}^{2\omega_0} \propto |\psi\rangle_{3/2}^{1/2} + |\psi\rangle_{1/2}^{1/2}. \tag{16}$$

The two GAM states of this coherent superposition are both eigenstates of the GAM operator $J_{z,1/2}$ (like the fundamental field) and therefore preserve the symmetry of the driving field, unlike their superposition. The reason is that these two GAMs are eigenstates of $J_{z,1/2}$ each with a different eigenvalue so that their superposition does not form an eigenstate of $J_{z,1/2}$. Physically, both field exhibit the same topology and spatially varying polarization distribution, as depicted in Fig. 1, but with a different azimuthal phase factor encoded by the nonlinear process. Consequently, their interferences will vary with the azimuthal angle, resulting in destructive interferences for $\theta = \pi$ which gives rise to the final crescent-shaped profile. It should be noted that the input field could also undergo spin-orbit coupling during its linear propagation through the inhomogeneous plasma. This effect arises from the spatial dependence of the plasma density distribution, leading to a non-zero divergence of the electric field. Similar to plasma-induced SHG, only fields that are eigenvectors of the total angular momentum (TAM) operator remain invariant during propagation in a circularly symmetric medium [45] (here, through the plasma) while in-

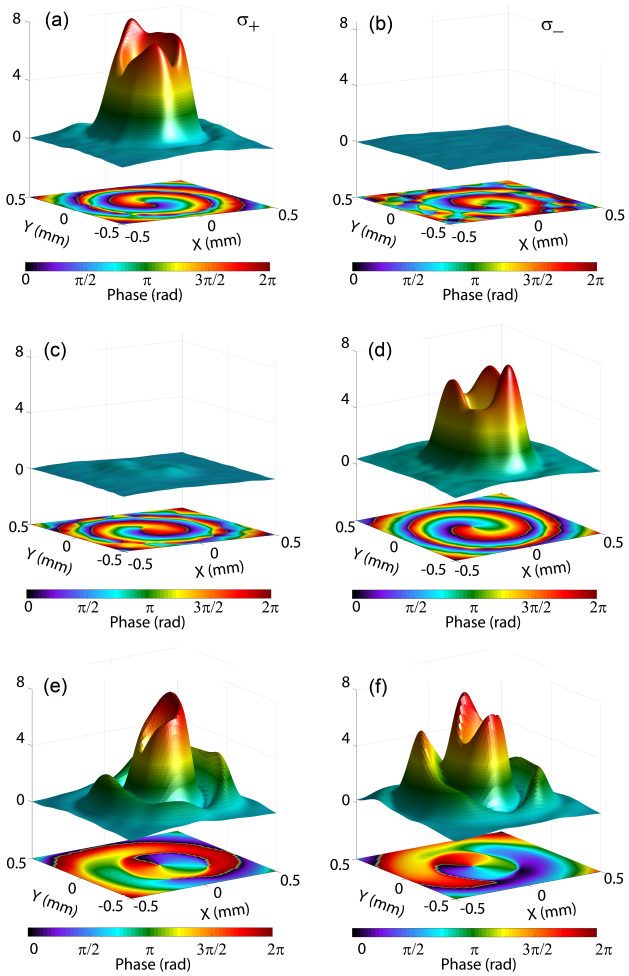

Figure 3 Circular decomposition of the SHG field driven by a fundamental field : $|\sigma_+\rangle$ ($\ell = 0$) in (a-b), $|\sigma_-\rangle$ ($\ell = 0$) in (c-d), and a radially polarized field $\frac{e^{-i\theta}|\sigma_+\rangle+e^{i\theta}|\sigma_-\rangle}{\sqrt{2}}$ in (e-f). The left (resp. right) column corresponds to the left (resp. right) circular component of the SHG field.

put fields with different polarization symmetry distributions (eigenvectors of the GAM with $\gamma \neq 1$) may undergo changes during propagation. However, this effect is of second-order and can be safely neglected due to the small thickness of the medium. The explicit symmetry breaking, highlighted in Fig. 5, is not limited to SHG driven by polarization Möbius strip, i.e. carrying half-integer GAM charge. Figure 6 displays the case of a twisted ribbon $|\psi\rangle_0^{-1} = \frac{e^{i\theta}|\sigma_+\rangle+e^{-i\theta}|\sigma_-\rangle}{\sqrt{2}}$ associated to the coordination parameter $\gamma = -1$ (eigenstate of $J_{z,-1}$ with the eigenvalue $j_\gamma = 0$). In this case as well, the output SHG field is modulated in amplitude, with 4 peaks observable in the inner part of the signal (associated with a modulation in $\cos[2\theta]$). The corresponding symmetry breaking is also explained by a SHG field built from the superposition of two GAM eigenstates of $J_{z,-1}$ which do not share the same eigenvalue $\vec{E}^{2\omega_0} \propto |\psi\rangle_2^{-1} + |\psi\rangle_{-2}^{-1}$.

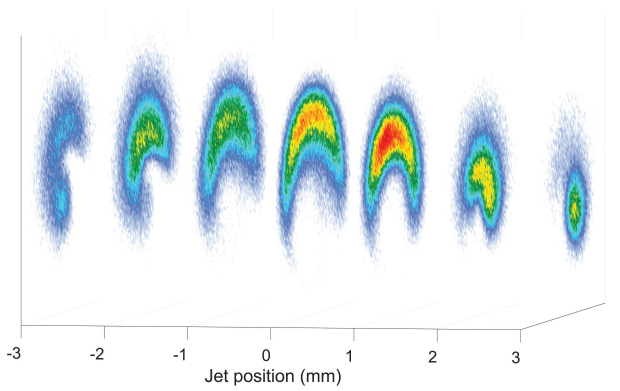

Figure 4 Intensity distribution of the SHG field generated by the GAM state $\frac{|\sigma_+\rangle+e^{i\theta}|\sigma_-\rangle}{\sqrt{2}}$ as a function of the position of the water jet with respect to the beam waist. Because of the ℓ dependent Gouy-phase, the produced SHG field rotates around the propagation axis.

In a general point of view, if one calculates the expectation value of the operator $J_{z,\gamma}$ for the produced SHG field, it gives:

$$\langle \vec{E}^{2\omega_0}|J_{z,\gamma}|\vec{E}^{2\omega_0}\rangle = 2j_\gamma, \tag{17}$$

revealing that, despite the lack of strict conservation, the GAM charge is nevertheless preserved *on average* through the plasma-induced SHG process. As far as the standard deviation is concerned, it reads

$$\sigma_{J_{z,\gamma}} = |\gamma - 1|. \tag{18}$$

This result highlights that the SHG field is a pure state only if the fundamental field is an eigenstate of the TAM (i.e., for $\gamma = 1$). For any other circumstances, the final state is a mixed state representing a coherent superposition of 2 GAM eigenstates that share the same coordination parameter γ as the pump, but with different eigenvalues breaking the GAM symmetry.

Although the GAM charge and the topology of the field are not preserved, the breaking of symmetry through the nonlinear process offers certain advantages. Firstly, the spatial beam profile of the SHG contains a signature of the topological properties of the driving field. As shown in Eq. 15, the SHG exhibits an amplitude modulation of the form $\cos[(\gamma-1)\theta]$ resulting in a beam profile with an even (resp. odd) number of peaks for γ integer (resp. half-integer). This property allows for easy differentiation between twisted ribbons and Möbius strips as driving fields. This result is linked to a recent demonstration [38] of direct characterization of light's OAM ℓ by measuring nonlocal photocurrent induced by nonlinear interaction. In the present work, the SHG from plasma currents provides information about the coordination parameter γ. Secondly, as previously discussed, the output SHG field involves a superposition of 4 quantum channels related to the pair of photons driving the nonlinear process (Eq. 11). It is possible to select the SHG produced from the crossed channels exclusively, i.e. the two photons of amplitude a_+a_-. This can be achieved,

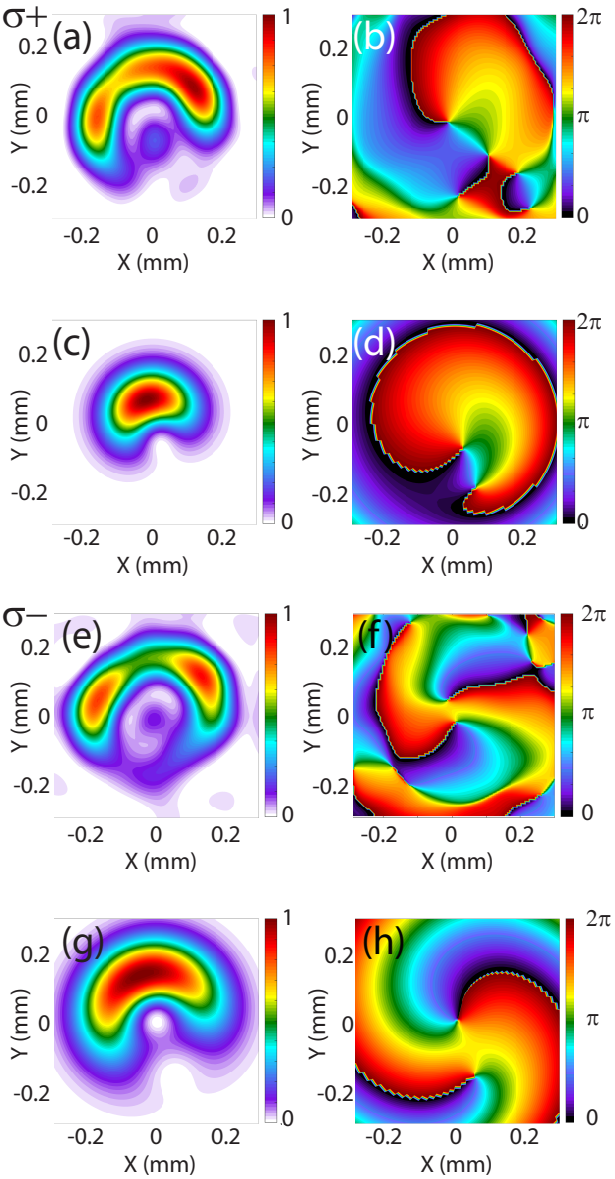

Figure 5 SHG field driven by a polarization Möbius strip $\frac{|\sigma_+\rangle+e^{i\theta}|\sigma_-\rangle}{\sqrt{2}}$. Left (resp. right) column corresponds to the spatial amplitude (resp. phase). The two first lines correspond to the SHG along the σ_+ component with the measurement in (a,b) and the corresponding simulation in (c,d). Similarly, panels (e,f) and (g,h) represent the experiment and the simulation for the σ_- component.

for instance, by implementing a noncollinear configuration with a small angle between the σ_+/σ_- beams and isolating the SHG generated along the bisector, as demonstrated in Ref. [36] Alternatively, the desired selection can also be obtained through a bi-color configuration with different frequencies ω_+/ω_- for the σ_+/σ_- components combined with a spectral selection (around the frequency $\omega_+ + \omega_-$) of the generated SHG field. From Eq. 11, the selection of these two specific quantum channels leads to a SHG field of the

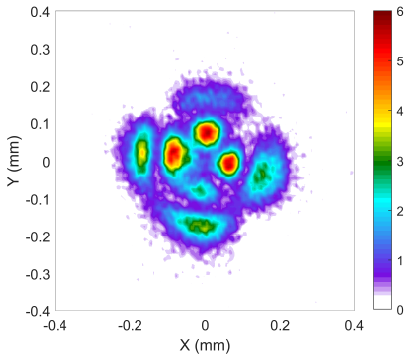

Figure 6 Intensity distribution of the SHG field driven by a polarization twisted ribbon $\frac{e^{i\theta}|\sigma_+\rangle+e^{-i\theta}|\sigma_-\rangle}{\sqrt{2}}$.

form:

$$\vec{E}^{2\omega_0} \propto a_+ a_- e^{i2j_\gamma\theta}\left(e^{i\theta}|\sigma_-\rangle + e^{-i\theta}|\sigma_+\rangle\right). \qquad (19)$$

By identifying this expression with the one of Eq. 3, one find a CR-invariant field $|\psi\rangle_{2j_\gamma}^{\gamma=1}$ eigenstate of J_z of eigenvalue $2j_\gamma$. As a result, regardless of the symmetry of the input field (e.g., twisted ribbons, Möbius strip, or even torus-knot topology), the harmonic field will always be produced along the coordination factor $\gamma = 1$, indicating that the nonlinear process acts as a topological attractor for the produced field. Moreover, it is noteworthy that the two components with opposite helicities in Eq. 19 will always be produced with equal amplitudes and phases, conferring a radial polarization pattern to the resulting SHG, irrespective of the driving field. Finally, one can notice that this robust topological attractor is produced along with a strict conservation of the GAM charge since one has $j_{\gamma=1}^{2\omega_0} = 2j_\gamma$. This universal trend in the generation of the SHG field can facilitate the characterization of the input GAM charge.

6. Conclusion

We have investigated the conservative nature of the GAM charge and the topology of light when up-converted photons are produced through a dipole-forbidden, quadrupole-allowed interaction. The nonlinear process in this study relies on the SHG produced by polarization Möbius strip and twisted ribbons in an isotropic inhomogeneous plasma. The non-linear medium is made of a thin jet of liquid water to avoid phase-matching limitations that could alter the spatial structure of harmonic signals. Following the anticipated conservation law, four quantum channels are allowed for the production of SHG. The resulting field can then be expressed as the superposition of two GAM states, each individually preserving the topology of the driving field but with different GAM charges. As a result, the GAM charge is shown to be conserved only on average and the total field exhibits an explicit symmetry breaking which aligns

well with our modeling approach. This symmetry breaking can be advantageously harnessed. The spatial profile of the generated harmonic field exhibits a dependence on the topology of the driving field so that one can readily differentiate driving fields having the topology of a twisted ribbon and Möbius strip. By selecting two specific quantum channels, it is also possible to produce a robust topological attractor for the SHG field that would be consistently generated with the coordination factor $\gamma = 1$ and conserving the GAM charge, regardless of the input field's topology. The present study highlights an array of other interesting prospects. The use of plasma for generating fields with non-trivial topology can be valuable as it avoids damage effects. In this context, a pump-probe configuration with a pump pulse for producing the plasma and a subsequent probe pulse inducing the SHG could offer greater flexibility. The generation of SHG depends on the plasma gradient and therefore on its spatial characteristics.Through a spatial shaping of the pump field, one could for instance manipulate the spatial distribution of the plasma enabling a fine control over the topological properties of the harmonic field with innovative functionalities. [38] The extension of the present investigation to polychromatic fields with the possibility of arbitrary fractional GAM charges could also lead to richer scenarios for exploration. Furthermore, investigating the sum- or difference-frequency generation in an homogeneous distribution of atoms or molecules by exploiting resonant quadrupole transitions [46] could constitute an interesting alternative platform for testing the impact of spin-orbit coupling with fields of non-trivial topologies. Finally, we emphasize the importance of understanding light-matter interactions with multiplexed light that combines both SAM and OAM. This plays a crucial role in the interplay between the chirality of light and matter, especially in scenarios involving nonlinear and multipolar interactions that align with the focus of the present study. Such a configuration has recently revealed the emergence of new forms of chiroptical spectroscopy and enantio-selectivity. [14]

Key words: orbital angular momentum, ultrashort optical vortex

References

[1] R. A. Beth, *Phys. Rev.* **1936**, *50*, 115.
[2] L. Allen, M. W. Beijersbergen, R. J. C. Spreeuw, and J. P. Woerdman, *Phys. Rev. A* **1992**, *45*, 8185.
[3] N. B. Simpson, K. Dholakia, L. Allen, and M.J. Padgett, *Opt. Lett.* **1997**, *22*, 52.
[4] E. Leader and C. Lorcé, *Physics Reports* **2014**, *541*(3), 163-248.
[5] L.-P. Yang, F. Khosravi, and Z. Jacob, *Phys. Rev. Res.* **2022**, *4*, 023165.
[6] S. Van Enk and G. Nienhuis, *J. Mod. Opt.* **1994**, *41*, 963.
[7] E. Noether, *Mathematisch-physikalische Klasse* **1918**, 235-257.
[8] V.S. Liberman and B. Ya. Zel'dovich, *Phys. Rev. A* **1992**, *46*, 5199-5207.
[9] K.Y. Bliokh, F.J. Rodríguez-Fortuño, F. Nori, and A.V. Zayats, *Nat. Phot.* **2015**, *9*, 796-808.
[10] Y. Shen, X. Wang, Z. Xie, C. Min, X. Fu, Q. Liu, M. Gong, and X. Yuan, *Light Sci. Appl.* **2019**, *8*, 90.
[11] A. Forbes, M. de Oliveira, and M. R. Dennis, *Nat. Phot.* **2021**, *15*, 253.
[12] S. Fürhapter, A. Jesacher, S. Bernet, and M. Ritsch-Marte, *Opt. Express* **2005**, *13*, 689
[13] K. A. Forbes and D. L Andrews, *JPhys. Photonics* **2021**, *3*, 022007.
[14] J.-L. Bégin, A. Jain, A. Parks, F. Hufnagel, P. Corkum, E. Karimi, T. Brabec, and R. Bhardwaj, *Nat. Phot.* **2023**, *17*, 82.
[15] R. Inoue, N. Kanai, T. Yonehara, Y. Miyamoto, M. Koashi, and M. Kozuma, *Phys. Rev. A* **2006**, *74*, 053809.
[16] D.-S. Ding, Z.-Y. Zhou, B.-S. Shi, and G.-C. Guo, *Nat. Comm.* **2013**, *4*, 2527.
[17] A. Nicolas, L. Veissier, L. Giner, E. Giacobino, D. Maxein, and J. Laurat, *Nat. Phot.* **2014**, *8*, 234.
[18] F. Trawi, F. Billard, O. Faucher, P. Béjot, and E. Hertz, *Laser Photonics Rev.* **2023**, *17* 2200525.
[19] A. Voisine, F. Billard, O. Faucher, P. Béjot, and E. Hertz, *Adv. Photonics Res.* **2024**, 2400008.
[20] H. He, M. E. J. Friese, N. R. Heckenberg, and H. Rubinsztein-Dunlop, *Phys. Rev. Lett.* **1995**, *75*, 826.
[21] Y. Yan, G. Xie, M. P. J. Lavery, H. Huang, N. Ahmed, C. Bao, Y. Ren, Y. Cao, L. Li, Z. Zhao, A. F. Molisch, M. Tur, M. J. Padgett, and A. E. Willner, *Nat. Comm.* **2014**, *5*, 4876.
[22] J. Wang, J.-Y. Yang, I. M. Fazal, N. Ahmed, Y. Yan, H. Huang, Y. Ren, Y. Yue, S. Dolinar, M. Tur, and A. E. Willner, *Nat. Phot.* **2012**, *6*, 488.
[23] P. Béjot and B. Kibler, *ACS Phot.* **2021**, *8*, 2345.
[24] P. Béjot and B. Kibler, *ACS Phot.* **2022**, *9*, 2066.
[25] H-J. Wu, H-R. Yang, C. Rosales-Guzmán, W. Gao, B-S. Shi, and Z-H. Zhu, *Phys. Rev. A* , *100*, 053840
[26] Y. Tang, K. Li, X. Zhang, J. Deng, G. Li, and E. Brasselet, *Nat. Photonics* **2020**, *14*, 658.
[27] G. Li, L. Wu, K. F. Li, S. Chen, C. Schlickriede, Z. Xu, S. Huang, W. Li, Y. Liu, E. Y. B. Pun, T. Zentgraf, K. W. Cheah, Y. Luo, S. Zhang, *Nano Lett.* **2017**, *17, 12*, 7974
[28] K. E. Ballantine, J. F. Donegan, and P. R. Eastham, *Sci. Adv.* **2016**, *2*(4), 1501748.
[29] E. J. Galvez, I. Dutta, K. Beach, J. J. Zeosky, J. A. Jones and B. Khajavi, *Sci. Rep.* **2017**, *7*, 13653.
[30] F. Wilczek, *Phys. Rev. Lett.* **1982**, *48*, 1144.
[31] E. Pisanty, G. J. Machado, V. Vicuna-Hernandez, A. Picon, A. Celi, J. P. Torres, and M. Lewenstein, *Nat. Phot.* **2019**, *13*, 569.
[32] A. de las Heras, A. K. Pandey, J. San. Roman, J. Serrano, E. Baynard, G. Dovillaire, M. Pittman, C. G.. Durfee, L. Plaja, S. Kazamias, O. Guilbaud, and C. Hernandez-Garcia, *Optica* **2022**, *9*(1), 71-79.
[33] C.-K. Huang, C. Zhang, Z. Nie, K. A. Marsh, C. E. Clayton, and C. Joshi, *Comm. Phys.* **2020**, *3*, 213.
[34] A. Turpin, L. Rego, A. Picon, J. San Roman, and C. Hernandez-Garcia, *Sci. Rep.* **2017**, *7*, 43888.
[35] E. Pisanty, L. Rego, J. San Roman, A. Picon, K. M. Dorney, H. C. Kapteyn, M. M. Murnane, L. Plaja, M. Lewenstein, and C. Hernandez-Garcia, *Phys. Rev. Lett.* **2019**, *122*, 2032001.
[36] M. Luttman, M. Vimal, M. Guer, J.-F. Hergott, A. Z. Khoury, C. Hernandez-Garcia, E. Pisanty, and T. Ruchon, *Sci. Adv.* **2023**, *9*(12), eadf3486.
[37] C. T. Schmiegelow, J. Schulz, H. Kaufmann, T. Ruster, U. G. Poschinger, and F. Schmidt-Kaler, *Nat. Comm.* **2016**, *7*(1), 12998.
[38] Z. Ji, W. Liu, S. Krylyuk, X. Fan, Z. Zhang, A. Pan, L. Feng, A. Davydov, and R. Agarwal, *Science* **2020**, *368*, 763-767.

[39] Y. R. Shen, *The Principles of Nonlinear Optics* (Wiley 1984).
[40] D. J. Hoffman, T. B. Van Driel, T. Kroll, C. J. Crissman, E. S. Ryland, K. J. Nelson, A. A. Cordones, J. D. Koralek, D. P. DePonte, *Chem. Phys. Lett.* **2003**, *376*(1), 214.
[41] C. Pan, H. Li, H. Pang, R. Ru, S. Zhang, D. Wei, H. Chen, H. Gao, F. Li, *Laser Photonics Rev.* **2023**, *18*, 2300625
[42] M. Beresna, P. G. Kazansky, Y. Svirko, M. Barkauskas, and R. Danielius, *Appl. Phys. Lett.* **2009**, *95*, 121502.
[43] R-Y. Zhong, Z-H. Zhu, H-J. Wu, C. Rosales-Guzman, S.-W. Song, and B-S. Shi, *Phys. Rev. A* **2021**, *103*, 053520.
[44] A. Rubano, F. Cardano, B. Piccirillo, and L. Marucci, *J. Opt. Soc. Am. B* **2019**, *36*(5), D70-D87.
[45] P. Béjot, *J. Opt. Soc. Am. B* **2024**, *41*(11), 1160-1169.
[46] D. S. Bethune,R. W. Smith, Y. R. Shen, *Phys. Rev. A* **1979**, *17*, 277

7. Acknowledgments

The authors gratefully acknowledge T. Ruchon for the careful reading of the manuscript and for providing valuable comments. This work was supported by the Conseil Régional de Bourgogne Franche-Comté, the CNRS, the EIPHI Graduate School (contract"ANR-17-EURE-0002") and has benefited from the facilities of the SMARTLIGHT platform in Bourgogne Franche-Comté (EQUIPEX+ contract "ANR-21-ESRE-0040"). H. Marroux has received funding from the European Research Council (ERC) under the European Union's [starting grant SATTOC (101078595)].